Model-based force and position tracking control of a multi-pressure hydraulic cylinder

Matti Linjama, Mikko Huova

Abstract

This paper presents a force control solution for a throttle-free multi-pressure hydraulic cylinder actuator. A model-based force controller was developed and the position and velocity tracking control was implemented using low-order linear controllers. Special attention was paid to robustness against variations in the load mass, bulk modulus and system delay. Experimental results demonstrated excellent energy efficiency and robustness, and acceptable tracking performance.

KEYWORDS: Hydraulics, multi-pressure actuator, force control, position control, robust control.

1 Introduction

Hydraulic cylinder actuators are used because of their efficient power density, endurance, and low cost. Increasing automation has created new demands for the controllability of cylinder actuators. Control is traditionally realized by four-way proportional or servo valves. These systems are nonlinear, which make them difficult to

control. Mattila et al. [1] surveyed the tracking control of hydraulic robot manipulators. They compared several solutions by using the ratio of peak position error to peak velocity as a performance index, and this index was also used in this paper. Kim et al. [2] used flatness-based non-linear control, Koivumäki and Mattila [3] used virtual decomposition control, and Won et al. [4] used the high-gain disturbance observer. The performance index is 3-5ms in the above-mentioned publications. Recently, the authors have studied the model-based force control of high inertia systems by using fast digital hydraulic valves.[5, 6] The inner-loop force controller linearizes the system and allows the use of simple controllers in the position and velocity loops. Special attention was paid to robustness against variations in bulk modulus, system delay and inertia. A simulation study with a simple system showed a performance index of 3ms [5] and the value was 9.5ms in another experimental system.[6] The main reason for the reduced performance in the latter system [6] was a large variation in the load mass, bulk modulus and system delay combined with simple P+PI outer-loop controllers.

The fundamental problem with the above-mentioned studies is that they are based on throttling control, which results in large energy losses. The combination of good energy efficiency and high performance control is difficult to achieve. Load sensing is the standard solution for mobile machinery, but the systems have relatively slow control valves and a tendency to oscillate. It is also well-known that energy efficiency is compromised in multi-actuator systems. Distributed valve systems reduce losses but

they often use quite slow proportional valves (see [7] and references therein). The approach was based on throttling control and losses were still significant. Linjama et al. [8] presented an alternative method, where a secondary controlled linear actuator was created by using a multi-chamber hydraulic cylinder. Energy losses were very small, but control was not good at lower velocities. Controllability of the multi-chamber cylinder can be improved by using slight throttling control, but energy losses increase.[9, 10] Multi-pressure systems are another way to implement energy efficient hydraulic actuation. The three-pressure system (two supply pressures plus a tank line) is the most common multi-pressure solution. Lumkes and Andruch [11] used a system with two variable supply pressures to control a multi-actuator system. Ketonen et al. [12] proposed a three-pressure system combined with digital hydraulic distributed valves for an excavator. Vucovic et al. [13] experimentally verified a three-pressure system in an excavator. The results showed improved productivity and reduced power losses. The above-mentioned multi-pressure systems used throttling control. A new proposition was to implement the multi-pressure system locally at the actuator, to increase the number of pressures, and to use throttle-free secondary control.[14, 15, 16] The benefit of this "hybrid actuator" approach was that it avoided high power transmission lines between the actuators. The challenge was the implementation: how to generate and maintain multiple pressure levels at the actuator. One solution presented in the above research [14, 15] integrated small converter cylinders into the actuator. Only one hydraulic

accumulator was used and converter cylinders were used to generate other pressures. In total six pressures were used to improve controllability of the system. Figure 1 shows the simplified hydraulic circuit diagram of the system. Each pressure level can be connected to either cylinder chamber via logic valves. The initial results of the system were promising. The power losses were very small—up to 77% lower than in traditional load sensing systems.[16] However, this number assumes that the energy returned to the tank line can be recovered and that crossflow is not used to improve controllability. The losses without tank line recovery and with the most advanced controller were still 64% lower than with load sensing systems. The control was based on the steady-state model and assumed instant pressure dynamics. The controllability was better than with the four-chamber cylinder used in Linjama, Vihtanen et al.'s [8] research because of the greater number of state combinations. However, there were some controllability problems at lower velocities and at certain state changes because dynamic effects were not considered.

This paper studies an alternative control approach for the system in Figure 1. The model-based dynamic force control approach presented by Linjama, Huova and Huhtala [5] is used. The same design methods can be used albeit the inner loop force controller is different. Chapter 2 presents the inner-loop force controller, which is the main contribution of this paper. Chapter 3 goes through the outer-loop controller and its tuning principles. An improved, robust controller is suggested for the position loop.

Chapter 4 presents the experimental system, Chapter 5 the controller tuning, and Chapter 6 the experimental results. Chapter 7 analyses the results and Chapter 8 gives conclusions.

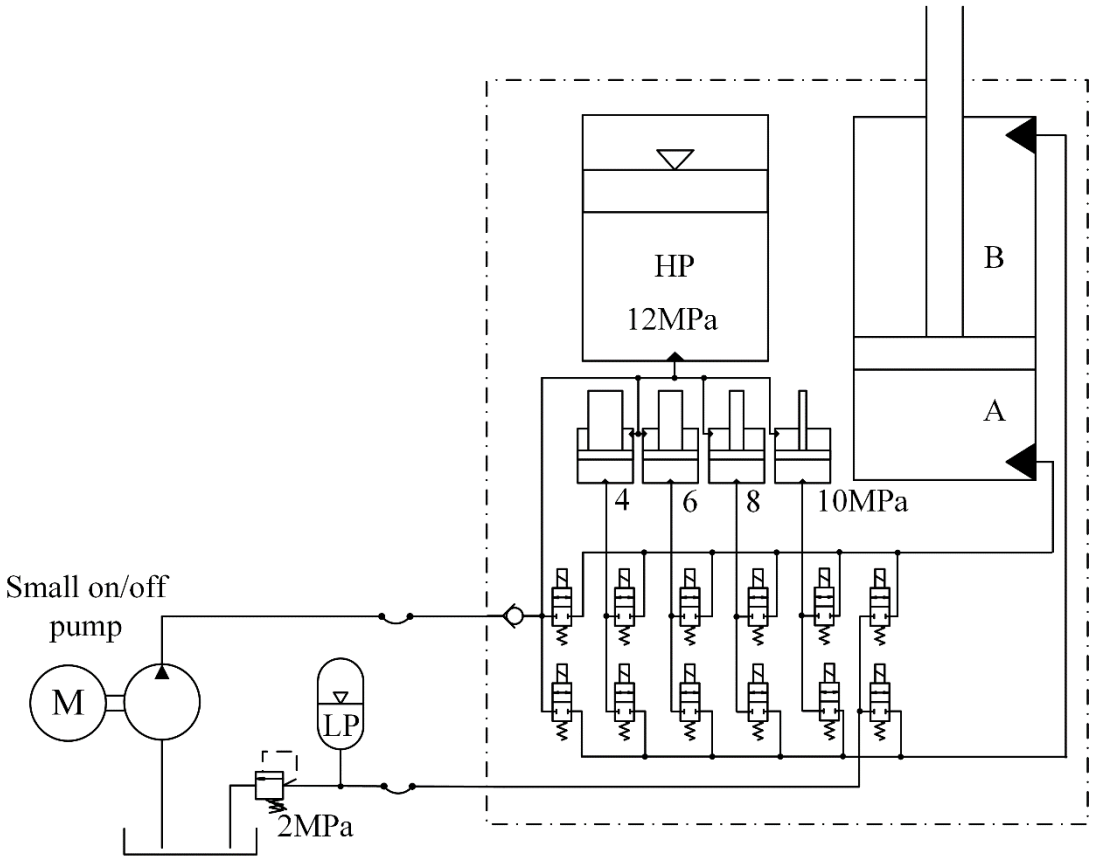

Figure 1. Principle of the multi-pressure hybrid actuator using one accumulator and small converter cylinders as pressure transformers.

2 Model-based force controller for multi-pressure system

2.1 System model

The dynamics of the system can be approximated by:

$$\begin{aligned}
\dot{p}_A &= \frac{B_{eff,A}(x)}{A_A x + V_{0,A} + V_{h,A}} \left(\sum_{i=1}^{6} Q_{A,i}\left(p_A, \mathbf{p_P}, \mathbf{u_A}\right) - A_A \dot{x} \right) \hat{=}\ f_A\left(p_A, x, \dot{x}, \mathbf{p_P}, \mathbf{u_A}\right) \\
\dot{p}_B &= \frac{B_{eff,B}(x)}{A_B\left(x_{max} - x\right) + V_{0,B} + V_{h,B}} \left(\sum_{i=1}^{6} Q_{B,i}\left(p_B, \mathbf{p_P}, \mathbf{u_B}\right) + A_B \dot{x} \right) \hat{=}\ f_B\left(p_B, x, \dot{x}, \mathbf{p_P}, \mathbf{u_B}\right) \\
m\ddot{x} &= A_A p_A - A_B p_B - F_\mu(\dot{x}) - F_{load}
\end{aligned} \tag{1}$$

where $\mathbf{p_P}$ is the vector of all six supply pressures and $\mathbf{u_A}$ and $\mathbf{u_B}$ are the vectors of control signals of the A- and B-side valves. Each flow path is implemented by two parallel-connected valves in order to reduce throttling losses and to improve controllability. The flow rates between pressure sources and cylinder chambers are:

$$\begin{aligned}
Q_{A,i}\left(p_A, \mathbf{p_P}, \mathbf{u_A}\right) &= \left(K_{v,A1,i} u_{A1,i} + K_{v,A2,i} u_{A2,i}\right) \sqrt[*]{p_{P,i} - p_A} \\
Q_{B,i}\left(p_B, \mathbf{p_P}, \mathbf{u_B}\right) &= \left(K_{v,B1,i} u_{B1,i} + K_{v,B2,i} u_{B2,i}\right) \sqrt[*]{p_{P,i} - p_B}
\end{aligned} \tag{2}$$

where $\sqrt[*]{\bullet}$ is used as a shortcut for the signed square root $\operatorname{sgn}(\bullet)\sqrt{|\bullet|}$. The control vectors for the A- and B-side valves are:

$$\begin{aligned}
\mathbf{u_A} &= \begin{bmatrix} u_{A1,1} & u_{A2,1} & u_{A1,2} & u_{A2,2} & u_{A1,3} & u_{A2,3} & u_{A1,4} & u_{A2,4} & u_{A1,5} & u_{A2,5} & u_{A1,6} & u_{A2,6} \end{bmatrix} \\
\mathbf{u_B} &= \begin{bmatrix} u_{B1,1} & u_{B2,1} & u_{B1,2} & u_{B2,2} & u_{B1,3} & u_{B2,3} & u_{B1,4} & u_{B2,4} & u_{B1,5} & u_{B2,5} & u_{B1,6} & u_{B2,6} \end{bmatrix}
\end{aligned} \tag{3}$$

The effective bulk moduli, $B_{eff,A}$ and $B_{eff,B}$, are solved using the following equations:

$$\frac{1}{B_{eff,A}(x)} = \frac{1}{B_{oil}} + \frac{V_{h,A}}{A_A x + V_{0,A} + V_{h,A}} \times \frac{1}{B_h}$$
$$\frac{1}{B_{eff,B}(x)} = \frac{1}{B_{oil}} + \frac{V_{h,B}}{A_B (x_{max} - x) + V_{0,B} + V_{h,B}} \times \frac{1}{B_h} \quad (4)$$

2.2 One step ahead estimator

The control principle is to estimate the state of the system after one sampling period and to select control signals so that the given cost function is minimized. The assumption is that the inertia of the system is so large that the piston velocity does not change significantly during one sampling period. This assumption decouples the differential equations of Equation 1, and pressures can be estimated without knowledge of the load mass. The single step Heun's method was used for the pressure estimation in the research of Linjama, Huova, et al. [5, 6] because very fast valves were used and the sampling period was short. In our case, the valves are significantly slower and better integration methods must be used. The pressure dynamics are fast and this is why a multistep approach was selected. The sampling period is divided into four parts and the multi-step Heun's method is used:

$$
\begin{aligned}
&\hat{p}_A(kT_s + h) = p_A(kT_S) + \frac{h}{2}(k_1 + k_2) \\
&k_1 = f_A\left(p_A(kT_S), x(kT_S), \dot{x}(kT_S), \mathbf{p_P}(kT_S), \mathbf{u_A}(kT_S)\right) \\
&k_2 = f_A\left(p_A(kT_S) + hk_1, x(kT_S) + h\dot{x}(kT_S), \dot{x}(kT_S), \mathbf{p_P}(kT_S), \mathbf{u_A}(kT_S)\right) \\
&h = T_S/4
\end{aligned}
\tag{5}
$$

It is assumed that piston velocity and supply pressures remain constant during one sampling period. The first step gives the estimate after quarter of the sampling period and the estimate after one sampling period is acquired by repeating Equation 5. The equations for the B-side pressure are similar. The estimator needs piston position and velocity, supply pressures and valve control signals as inputs. Only the highest and lowest supply pressures are measured and the middle pressures are calculated from the highest pressure according to the piston area ratios of the converter cylinders.

2.3 Force controller

The purpose of the force controller is to select the control signals that minimize force error. This is done by estimating pressures after one sampling period using Equation 5 and selecting the best control signal for the next sampling period. There are several contradictory requirements that must be taken into account:

1) Force error should be small.
2) Energy losses of the system should be small.
3) Activity of the valves should be moderate.

4) Pistons of the converter cylinders should not achieve the end positions.

2.3.1 Search space

The system has 24 valves and thus 2^{24} different states. The essential step is to define a reduced set of states—the so-called search space—in order to achieve real-time control of the system. The selected A- and B-side search spaces are identical and include one valve open, two valves open and three valves open. The state where one valve is open allows a slower increase or decrease of the pressure. Opening both parallel-connected valves results in a faster pressure change rate. The crossflow between the two adjacent pressure sources is used to improve controllability and is implemented by 1+1 or 1+2 valves. The search spaces for the A-side and B-side valves are:

$$\mathbf{SS_A} = \mathbf{SS_B} = \begin{bmatrix}
0 & 0 & 0 & 0 & 0 & 0 & 0 & 0 & 0 & 0 & 0 & 0 \\
1 & 1 & 0 & 0 & 0 & 0 & 0 & 0 & 0 & 0 & 0 & 0 \\
0 & 0 & 1 & 1 & 0 & 0 & 0 & 0 & 0 & 0 & 0 & 0 \\
0 & 0 & 0 & 0 & 1 & 1 & 0 & 0 & 0 & 0 & 0 & 0 \\
0 & 0 & 0 & 0 & 0 & 0 & 1 & 1 & 0 & 0 & 0 & 0 \\
0 & 0 & 0 & 0 & 0 & 0 & 0 & 0 & 1 & 1 & 0 & 0 \\
0 & 0 & 0 & 0 & 0 & 0 & 0 & 0 & 0 & 0 & 1 & 1 \\
1 & 0 & 0 & 0 & 0 & 0 & 0 & 0 & 0 & 0 & 0 & 0 \\
0 & 0 & 1 & 0 & 0 & 0 & 0 & 0 & 0 & 0 & 0 & 0 \\
0 & 0 & 0 & 0 & 1 & 0 & 0 & 0 & 0 & 0 & 0 & 0 \\
0 & 0 & 0 & 0 & 0 & 0 & 1 & 0 & 0 & 0 & 0 & 0 \\
0 & 0 & 0 & 0 & 0 & 0 & 0 & 0 & 1 & 0 & 0 & 0 \\
0 & 0 & 0 & 0 & 0 & 0 & 0 & 0 & 0 & 0 & 1 & 0 \\
0 & 1 & 1 & 0 & 0 & 0 & 0 & 0 & 0 & 0 & 0 & 0 \\
0 & 0 & 0 & 1 & 1 & 0 & 0 & 0 & 0 & 0 & 0 & 0 \\
0 & 0 & 0 & 0 & 0 & 1 & 1 & 0 & 0 & 0 & 0 & 0 \\
0 & 0 & 0 & 0 & 0 & 0 & 0 & 1 & 1 & 0 & 0 & 0 \\
0 & 0 & 0 & 0 & 0 & 0 & 0 & 0 & 0 & 1 & 1 & 0 \\
1 & 1 & 1 & 0 & 0 & 0 & 0 & 0 & 0 & 0 & 0 & 0 \\
0 & 1 & 1 & 1 & 0 & 0 & 0 & 0 & 0 & 0 & 0 & 0 \\
0 & 0 & 1 & 1 & 1 & 0 & 0 & 0 & 0 & 0 & 0 & 0 \\
0 & 0 & 0 & 1 & 1 & 1 & 0 & 0 & 0 & 0 & 0 & 0 \\
0 & 0 & 0 & 0 & 1 & 1 & 1 & 0 & 0 & 0 & 0 & 0 \\
0 & 0 & 0 & 0 & 0 & 1 & 1 & 1 & 0 & 0 & 0 & 0 \\
0 & 0 & 0 & 0 & 0 & 0 & 1 & 1 & 1 & 0 & 0 & 0 \\
0 & 0 & 0 & 0 & 0 & 0 & 0 & 1 & 1 & 1 & 0 & 0 \\
0 & 0 & 0 & 0 & 0 & 0 & 0 & 0 & 1 & 1 & 1 & 0 \\
0 & 0 & 0 & 0 & 0 & 0 & 0 & 0 & 0 & 1 & 1 & 1
\end{bmatrix}$$

Zero state

Control using two valves

Control using a single valve

Crossflow using 1+1 valves

Crossflow using 2+1 valves

(6)

Both search spaces have 28 elements. The final search space is obtained by forming all 28^2 combinations.

2.3.2 Cost function and optimal output

The balance between different objectives is achieved by defining a cost function, which is the weighted sum of all the unwanted phenomena. The cost function used is:

$$J = \left| F_{ref} - \left(A_A \hat{p}_A - A_B \hat{p}_B \right) \right| + W_{sw} N_{sw} + W_{loss} E_{loss} + W_{conv} \sum_{i=1}^{4} Q_{conv,i} x_i^3 \quad (7)$$

where $\hat{p}_A$ and $\hat{p}_B$ are the estimated pressures for the new state (using Equation 5), N_{sw} is the number of valve switches needed to shift from the current state to the new state, and the energy loss, E_{loss}, is calculated as follows:

$$E_{loss} = \frac{T_S}{2} \left(P_{loss}\left(kT_S\right) + P_{loss}\left(\left(k+1\right)T_S\right) \right) \quad (8)$$

where the power loss, P_{loss}, consists of the hydraulic losses of the all control valves, i.e. the product of the flow rate and pressure differential over the valve. The power loss, $P_{loss}(kT_S)$, is calculated by using the new state and actual pressures, while $P_{loss}((k+1)T_S)$ is calculated by using the new state and estimated new pressures. The last term of the cost function sets the penalty for the state of the converter cylinders. The x_i is the deviation of the piston i from the centre position, and $Q_{conv,i}$ is the calculated flow rate towards piston i.

The value of the cost function is increased by 10^6N if the estimated pressure is below p_{min} or above p_{max}. The value of the cost function is evaluated for all 28^2 control

combinations of the search space. The control combination that gives the smallest value is selected as the controller output.

2.3.3 Stop motion logic

Stop motion logic is implemented in order to reduce activity of the valves when the piston does not move. The logic is similar to that presented in the study by Linjama et al.[8] All valves are closed if the following conditions hold:

$$\begin{aligned} &\left|x_{ref}-x\right| \le x_{tol1} \text{ AND} \\ &\left|v_{ref}\right| \le v_{tol} \end{aligned} \tag{9}$$

The force controller is enabled again if one of the following conditions holds:

$$\begin{aligned} &\left|x_{ref}-x\right| > x_{tol2} \text{ OR} \\ &\left|v_{ref}\right| > v_{tol} \end{aligned} \tag{10}$$

2.4 Force dynamics under uncertain bulk modulus

It is shown in the study by Linjama, Huova and Huhtala [5] that the force dynamics under certain assumptions can be approximated by:

$$F(s) = \frac{\frac{\tau_B A_A + \tau_A A_B}{A_A + A_B}s + 1}{(\tau_A s + 1)(\tau_B s + 1)} F_{ref}(s) \hat{=} G_F(s) F_{ref}(s) \tag{11}$$

where τ_A and τ_B are the time constants of the pressure dynamics:

$$\tau_A = -\frac{T_S}{\ln\left(1 - B_{eff,A}/\hat{B}_{eff,A}\right)},\ \tau_B = -\frac{T_S}{\ln\left(1 - B_{eff,B}/\hat{B}_{eff,B}\right)} \quad (12)$$

and B_{eff} is the actual effective bulk modulus, and $\hat{B}_{eff}$ is its estimate. Equations 11 and 12 are valid if chamber pressures are controlled, pressure controllers work perfectly and pressure references are selected as in the Linjama, Huova and Huhtala study.[5] In our case, the assumptions are not valid because chamber pressures are not controlled—target pressures are not present in Equation 7. It was shown that Equation 11 is a good approximation for the force dynamics in this case as well. This is done by simulating the frequency responses of the force controller and comparing them to the frequency response of $G_F(s)$. Figure 2 shows the simulation model. The system parameters are given in Figure 4 and Table 1, and the controller parameters in Table 2.

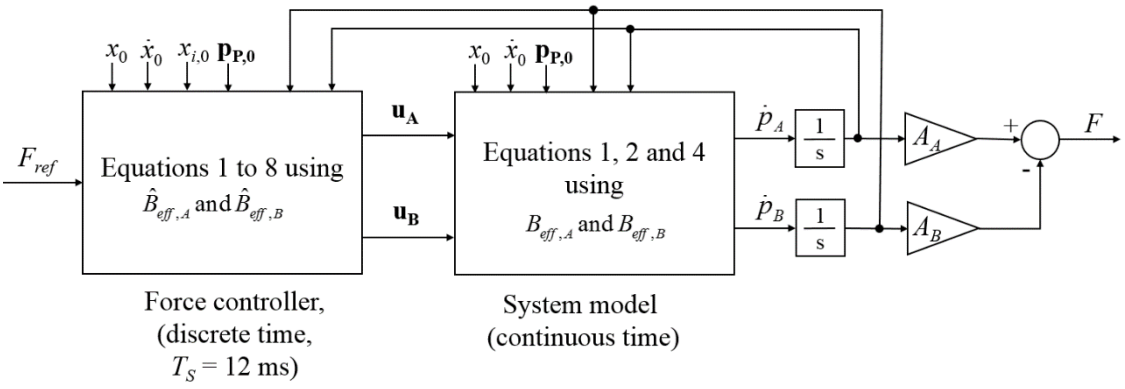

Figure 2. Block diagram of the simulation model used in the simulation of the frequency responses of the force controller.

The simulations are performed at the operation point

$x = x_0, \dot{x} = \dot{x}_0\ p_A = p_{A,0}, x_i = x_{i,0}, \mathbf{p_P} = \mathbf{p_{P,0}}$. The load force is assumed to be zero and the initial value for p_B is calculated from the force balance equation. The uncertainty in the bulk modulus is assumed to be solely in the bulk modulus of oil B_{oil}. Thus, there are 14 variables, which make the simulation study demanding. In order to reduce the number of simulations, supply pressures and piston positions of the converter cylinders are assumed to be constant. The parameter values are:

$$
\begin{aligned}
&\mathbf{p_{P,0}} = \begin{bmatrix} 2 & 4.4 & 6.8 & 9.2 & 11.6 & 14 \end{bmatrix} \text{ MPa} \\
&x_{i,0} = 0 \\
&x_0 = \{0.15, 0.25\} \text{ m} \\
&\dot{x}_0 = \{-0.1, 0, 0.1\} \text{ m/s} \\
&p_{A,0} = \{1, 1.55, 2.1, \ldots, 10.9, 11.45, 12\} \text{ MPa} \\
&B_{oil} = \{800, 1200\} \text{ MPa} \\
&\hat{B}_{oil} = 1400 \text{ MPa}
\end{aligned}
\tag{13}
$$

The input signal to the simulation model is a sinusoidal force reference with ±10kN amplitude. The least-squares method is used to fit the sinusoidal signal to the simulated output force, and the amplitude ratio and phase shift are determined from the input- and output-fitted signals. The algorithm does not always find the correct fit, and corresponding points are not plotted in the Bode diagrams. Figure 3 shows a comparison of the simulated and theoretical Bode diagrams. A delay of half of the sampling period is added to $G_F(s)$ in order to consider sampling. Some variation in the

frequency response is seen when parameters are varied. In general, $G_F(s)$ plus delay is a relatively good linear model for the force controller.

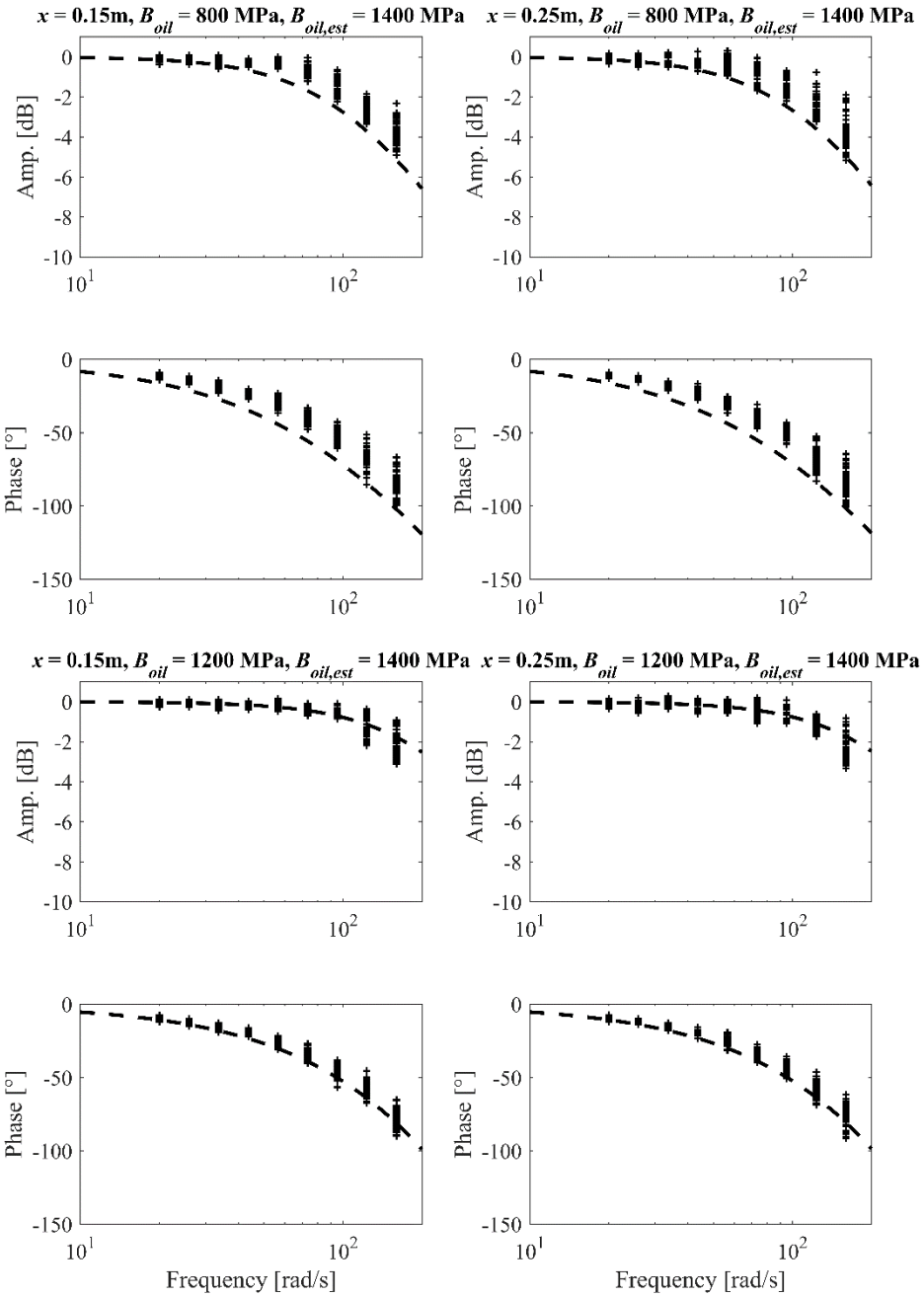
x = 0.15m, B_oil = 800 MPa, B_oil,est = 1400 MPa
x = 0.25m, B_oil = 800 MPa, B_oil,est = 1400 MPa
x = 0.15m, B_oil = 1200 MPa, B_oil,est = 1400 MPa
x = 0.25m, B_oil = 1200 MPa, B_oil,est = 1400 MPa
Amp. [dB]
Phase [°]
Frequency [rad/s]

Figure 3. Simulated and theoretical frequency responses with different values for piston position and bulk modulus of oil. Other parameters vary according to Equation 13. Theoretical responses are shown in broken line.

3 Robust motion controller

3.1 System uncertainties

The design of the outer loop position and velocity controllers is similar to that presented in the Linjama, Huova and Huhtala study.[5] The analysis presented in Section 2.4 shows that the force controller approximates the dynamics $G_F(s)$ plus delay caused by sampling. The time constants depend on the piston position and the unknown bulk modulus of oil. The real system has additional delay caused by the control valves and computation. The valve delay depends on factors such as the pressure, oil viscosity and coil temperature, and is thus a partly unknown variable. The third unknown variable is the load mass. The system also has high frequency dynamics caused by pipelines, for example, and the controller must be robust against such uncertainties.

3.2 Velocity controller

If the bulk modulus of the oil is close to its estimate, the time constants τ_A and τ_B are small and $G_F(s)$ approaches unity gain. The nominal open-loop model from the force reference to the velocity is selected to be:

$$G_{N,vel}(s) = \frac{1}{m_{min} s} e^{-(T_S/2 + d_{min})s} \tag{14}$$

where d_{min} is the smallest valve delay and m_{min} is the minimum load mass. The true transfer function is:

$$G_{T,vel}(s) = \frac{1}{m s} G_F(s) e^{-(T_S/2 + d)s} \tag{15}$$

where m is the actual load mass and d is the actual valve delay plus computational delay. The multiplicative modelling error caused by the parameter variations is:

$$\Delta_{vel}(s) = \frac{G_{T,vel}(s) - G_{N,vel}(s)}{G_{N,vel}(s)} \tag{16}$$

The system remains stable if $G_{T,vel}$ and $G_{N,vel}$ have the same number of unstable poles, and the following holds [17]:

$$\left|\Delta_{vel}(j\omega)\right| < \left|\frac{1 + G_{N,vel}(j\omega) G_V(j\omega)}{G_{N,vel}(j\omega) G_V(j\omega)}\right| \quad \forall \omega > 0 \tag{17}$$

where G_V is the transfer function of the velocity controller. The design problem is to find such $G_V(s)$ that the nominal system is stable and Equation 17 is satisfied with all parameter values. In practice, some margin is required in Equation 17 in order to have a non-oscillatory response with all parameter values, and this margin should increase with the frequency in order to have robustness against unmodelled high-frequency dynamics.

It was shown in the study by Linjama, Huova and Huhtala [5] that a simple P-controller is a good candidate for the velocity controller:

$$G_V(s) = K_{P,vel} \tag{18}$$

3.3 Position controller

The nominal and true open-loop transfer functions of the position loop are obtained by closing the velocity loop:

$$G_{N,pos}(s) = \frac{G_{N,vel}(s)G_V(s)}{s\left(1+G_{N,vel}(s)G_V(s)\right)}\ ,\ G_{T,pos} = \frac{G_{T,vel}(s)G_V(s)}{s\left(1+G_{T,vel}(s)G_V(s)\right)} \tag{19}$$

The multiplicative modelling error is calculated similarly to Equation 16:

$$\Delta_{pos}(s) = \frac{G_{T,pos}(s) - G_{N,pos}(s)}{G_{N,pos}(s)} \tag{20}$$

and the system remains stable if the following holds:

$$\left|\Delta_{pos}(j\omega)\right| < \left|\frac{1+G_{N,pos}(j\omega)G_P(j\omega)}{G_{N,pos}(j\omega)G_P(j\omega)}\right| \ \forall \omega > 0 \tag{21}$$

where $G_P(s)$ is the transfer function of the position controller. The PID controller was suggested as a position controller in Linjama, Huova and Huhtala's study [5] but tests have shown that the D-term is not beneficial in practice.[6] The PI(D) controller results

in quite a large overshoot and a moderate position tracking performance. An alternative five-parameter controller is suggested in this paper:

$$G_P(s) = K_{P,pos} \times \frac{s^2/\omega^2 + 2\xi s/\omega + 1}{(\tau s + 1)^2} + \frac{K_{I,pos}}{s} \quad (22)$$

The parameters ω, ξ and τ are used to shape the right hand side of Equation 21 to fit better with the uncertainty.

4 Experimental system

Figure 4 shows the test system and its hydraulic circuit diagram. The system parameters are given in Figure 4 and in Table 1. The exact values of the dead volumes and the bulk modulus of hose were not known but the values were used by the controller, and for analysis and simulations. The boom length was four meters and the exact dimensions of the boom mechanism were given by Huova et al.[16] Linear potentiometers were used to measure the positions of the main cylinder and converter cylinders. The control hardware consisted of a dSPACE DS1006 controller board together with a DS2002 ADC board, a DS3001 incremental encoder board and a DS4302 CAN interface board. The flow rates were measured directly from pulses using the DS3001 board. The valves were controlled via a CAN bus with pulse-width modulated power electronics. The supply voltage was 48VDC and when the valve was opened, the duty cycle was 100% for the first 6 milliseconds and 25% thereafter. Valve closing was implemented by

feeding -48VDC to the coil until the current was zero. The pump was enabled when the pressure dropped below 14 MPa and disabled when pressure raised above 15 MPa. The pressures in the converter piston chambers were measured, but not used, by the controller.

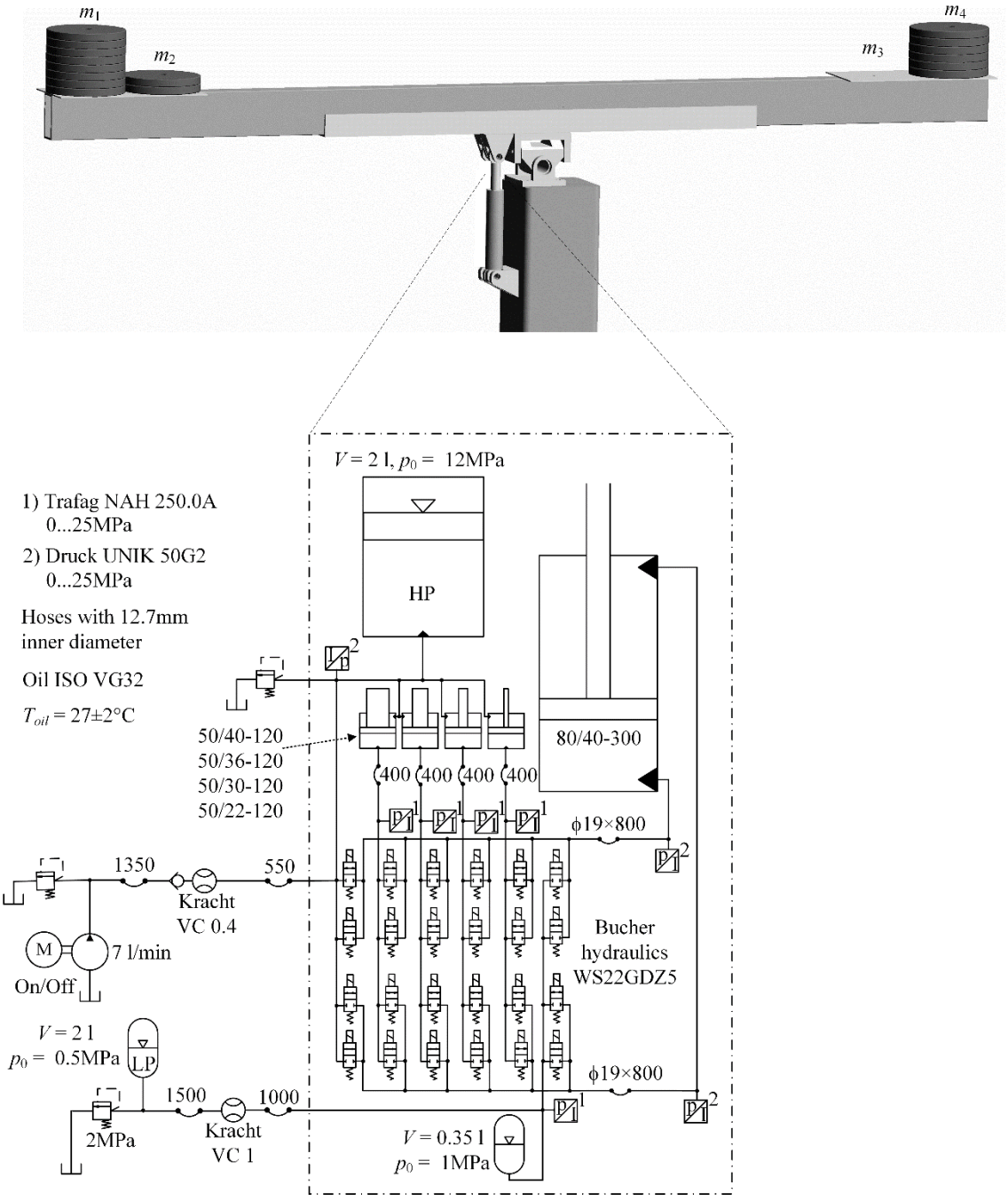

Figure 4. Hydraulic circuit diagram of the experimental setup.

Table 1. System parameters.

$V_{0,A}$	0.4	Dead volume, A-side [dm^3]
$V_{0,B}$	0.4	Dead volume, B-side [dm^3]
$V_{h,A}$	$\pi/4\times0.019^2\times0.8$	Hose volume, A-side [m^3]
$V_{h,B}$	$\pi/4\times0.019^2\times0.8$	Hose volume, B-side [m^3]
$K_{v,A1,i}$ & $K_{v,A2,i}$	2.357×10^{-7}	Flow coefficients of A-side valves [$m^3s^{-1}Pa^{-0.5}$]
$K_{v,B1,i}$ & $K_{v,B2,i}$	2.357×10^{-7}	Flow coefficients of B-side valves [$m^3s^{-1}Pa^{-0.5}$]
B_h	600	Bulk modulus of hose [MPa]

5 Controller tuning

5.1 Range of parameters

The effective inertia of the system depends on the load masses and boom orientation. The maximum effective inertia is about 49000kg in the horizontal orientation and is achieved when load mass is 400kg in total. The minimum inertia is assumed to be half of this—24500kg. The valve delay is assumed to vary between 5ms and 8ms. The sampling period is 10ms and the computational delay is measured to be below 1ms. These values give a system delay of between 10ms and 14ms. The bulk modulus of oil is assumed to be between 800MPa and 1400MPa and the estimate of the bulk modulus of oil is selected to be 1400MPa. The smallest value of the time constants τ_A and τ_B is

thus 0ms and the highest values can be calculated by Equations 4 and 12. The highest values are 12.2ms for τ_A and 11.9ms for τ_B.

5.2 Measurement signal management

The controller uses filtered signals in order to reduce sensitivity to measurement noise. The pressure and position signals are filtered with a three-point median filter. After that, signals are filtered with a first order digital filter. The time constants are 4.5ms for chamber pressures, 12ms for piston position, and 24ms for supply pressure, tank pressure and converter piston positions. The filtered converter piston positions are fed through a backlash block with a 0.1mm backlash width. The velocity signal needed by the controller is differentiated from the filtered position by using the filter suggested by Harrison and Stoten:[18]

$$\dot{x}(k) \approx \frac{5x(k)+3x(k-1)+x(k-2)-x(k-3)-3x(k-4)-5x(k-5)}{35T_{S,\,fast}} \tag{23}$$

All filters run with the sampling period of $T_{S,fast}$ = 0.5ms.

5.3 Outer-loop velocity and position controllers

The tuning of the outer-loop controllers is made in continuous time and they are discretized by using Tustin's approximation. The tuning of the outer-loop velocity controller is done by plotting both sides of Equation 17 with different parameter values and by finding a suitable value for $K_{P,vel}$. The suitable value is determined visually by

inspecting the margin between curves and step responses with different parameter values. The resulting gain value is $K_{P,vel}$ = 700 kN s m^{-1}. Figure 5 presents both sides of Equation 17 and the closed-loop velocity step responses of the linear model. The tuning of the outer-loop position controller is done similarly, by plotting both sides of Equation 21 with different parameter values and by finding suitable values for the parameters. The resulting tuning is $K_{P,pos}$ = 13s^{-1}, $K_{I,pos}$ = 22s^{-2}, ω = 42 rad/s, ξ = 0.55 and τ = 6ms. Figure 5 shows both sides of Equation 21 and the closed-loop position step responses of the linear model.

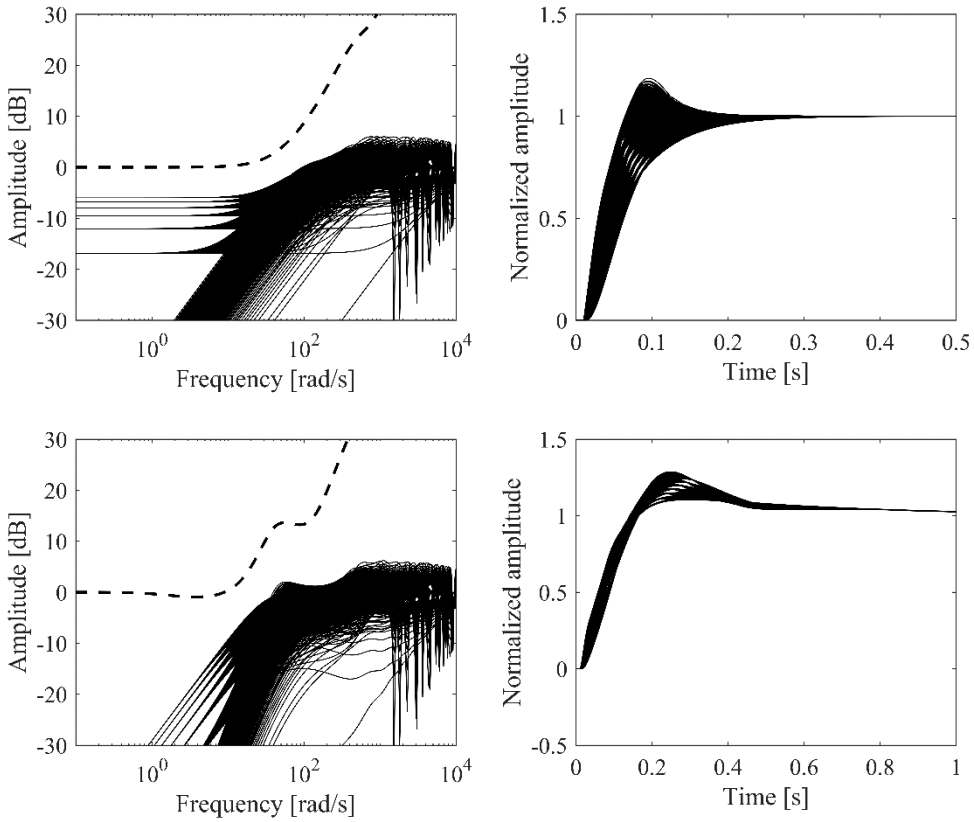

Figure 5. Both sides of Equation 17 (top left) and corresponding velocity step responses of the linear model (top right). Both sides of Equation 21 (bottom left) and corresponding position step responses of the linear model (bottom right). The parameters have seven equally spaced values within the ranges m = 24500–49000kg, system delay = 11–21.5ms, τ_A = 0.1–12.2ms, and τ_B = 0.1–11.9ms.

5.4 Inner-loop force controller

The initial tuning of the inner-loop force controller is done by simulating a smooth position trajectory and observing position, velocity and force tracking errors, and converter piston positions. The supply pressures are assumed to be constant and values are given by Equation 13. Final tuning is done in the real system. The tuning principle is to first find the value for W_{conv} such that the converter pistons do not hit the end positions. Then, W_{loss} and W_{sw} are tuned such that energy consumption and activity of valves is minimized without too large position and force tracking errors. The peak position error divided by peak velocity is used as a performance index for position error, and the integral of the squared force error is used as a performance error for the force tracking. Responses are measured ten times in order to find the average values. The resulting tuning parameters are given in Table 2. It is important to note that the tuning is the trade-off between different objectives.

Table 2. Controller parameters.

T_S	0.010	Sampling period (s). Should be longer than valve delay.
$T_{S,fast}$	0.0005	Fast sampling period (s). Used for data acquisition and filtering.
$K_{P,vel}$	700000	Velocity controller gain (N s m^{-1})

$K_{P,pos}$	13	Position controller gain, P-term (s^{-1})
$K_{I,pos}$	22	Position controller gain, I-term (s^{-2})
ω	42	Tuning parameter of the position controller (rad/s)
τ	0.006	Tuning parameter of the position controller (s)
ξ	0.55	Tuning parameter of the position controller (-)
deadzone	0.0007	Integrator dead zone (m). Integrator is disabled when position error is below *deadzone*.
W_{sw}	100	Weight for valve switching (N/switching)
W_{loss}	80	Weight for energy losses (N/J)
W_{conv}	2×10^{11}	Weight for converter piston position (N s/m^6)
p_{min}	0.5	Lowest allowed chamber pressure (MPa)
p_{max}	16	Highest allowed chamber pressure (MPa)
v_{tol}	0.0001	Stopping tolerance for velocity reference (m/s)
x_{tol1}	0.0005	Stopping tolerance for piston position error (m)
x_{tol2}	0.0007	Stopping tolerance for piston position error (m)

6 Experimental results

Figure 6 shows the measured response of the system when the load masses are m_1 = 125kg, m_2 = 0kg, m_3 = 0kg and m_4 = 25kg (see Figure 4). The effective inertia was about 24500kg on the horizontal orientation. The position reference was a fifth order

polynomial with 35mm and 70mm amplitudes and a 1.25s movement time, giving peak velocities of 52.5mm/s and 105mm/s. The uppermost plot shows the measured piston position together with the position reference. The following plots present the position error, the velocity differentiated from the measured position together with the velocity reference, the measured chamber pressures, the force reference and force calculated from the chamber pressures, the force error, the states of A- and B-side valves, and the piston positions of the converter cylinders, respectively. The differentiated velocity was filtered twice by a second order filter with damping factor of 0.7 and cut-off frequency of 100 Hz before plotting. The force error was plotted only when the controller was active. The A- and B-side valve states are expressed as the row index of the matrix of Equation 5 with one subtracted. The plots also show two horizontal lines. If the state was above the upper line, crossflow was used. If the state was between the lines, only one valve was controlled and if the state was below the lower line, both parallel-connected valves were controlled.

Figure 7 shows the measured response when load masses were changed to m_1 = 200kg, m_2 = 50kg, m_3 = 0kg and m_4 = 150kg (see Figure 4). The effective inertia was about 49000kg in the horizontal orientation. The tracking error and overshoot increased, but the response was smooth and stable.

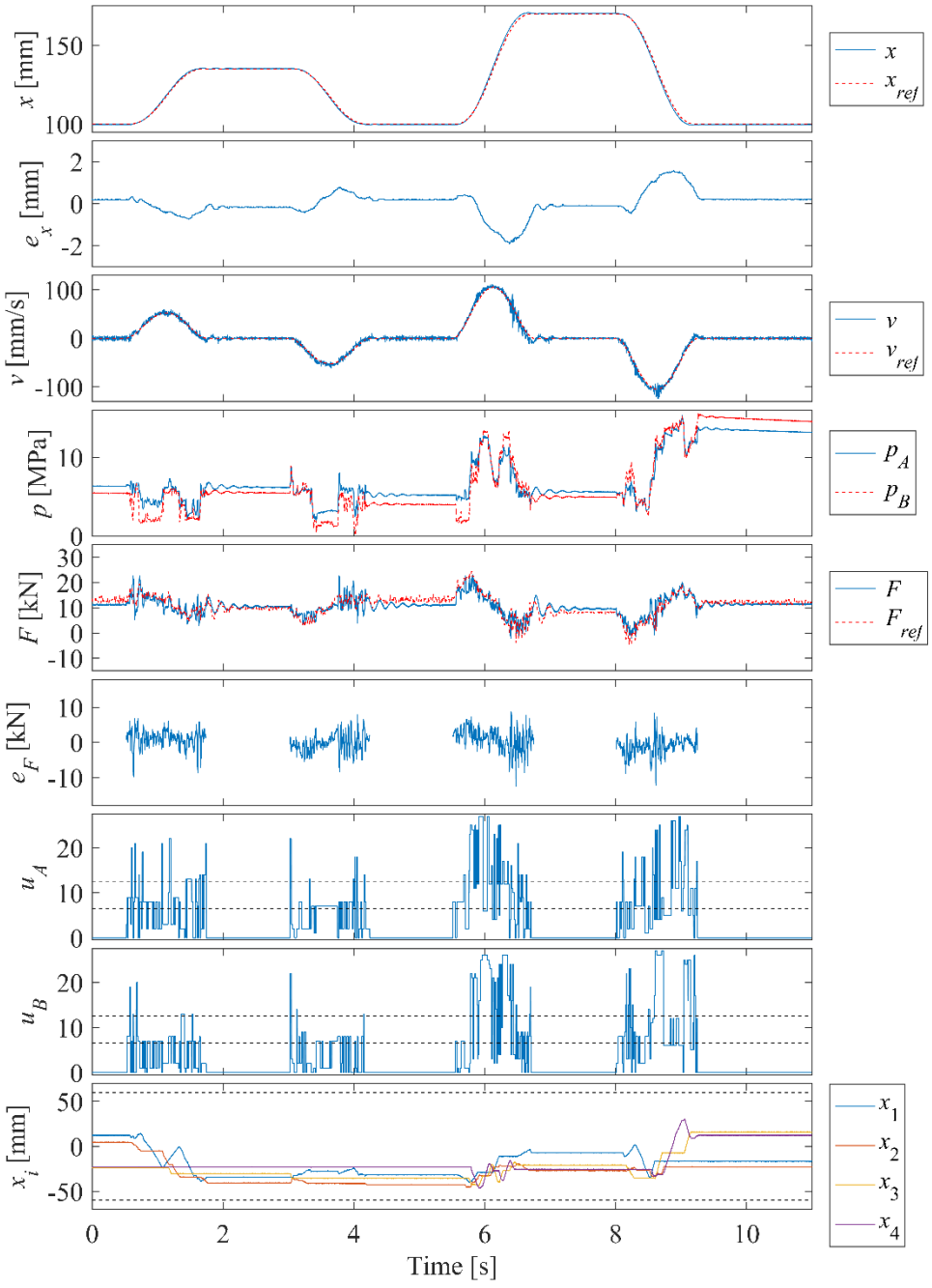

Figure 6. Measured response with 24500kg effective inertia.

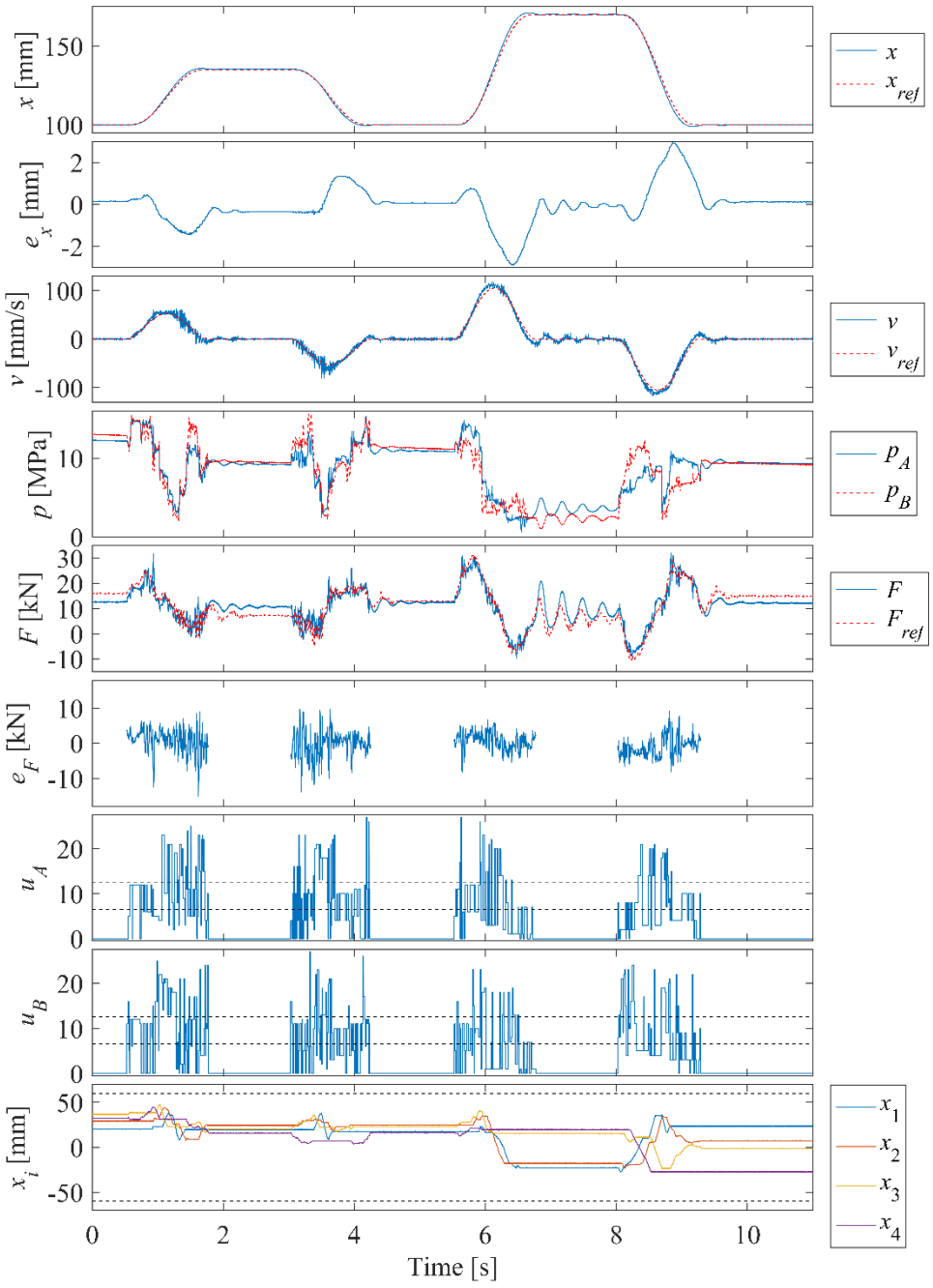

Figure 7. Measured response with 49000kg effective inertia.

7 Analysis of results

7.1 Energy efficiency

The mechanical power output of the system can be calculated as a product of piston velocity and piston force. The force is calculated from the measured chamber pressures. The input power is calculated as a product of pump flow and the highest supply pressure. Power loss is the difference between the input and output power, and energy loss is obtained by integration. It is assumed that the energy returned to the tank line cannot be recovered. The energy loss depends on the state of the converter pistons and the pump control sequence, and thus varies from one movement to another. The movements shown in Figures 6 and 7 were repeated 20 times in order to determine the average energy loss. The average loss was 19.5J/mm for the 24500kg effective inertia and 18.9J/mm for the 49000kg inertia. These are good values, because the loss value for the same system with electric load sensing and a mobile proportional valve was 45J/mm, with electric load sensing and distributed digital hydraulic valves it was 29J/mm,[19] and with the secondary controlled multi-chamber cylinder it was about 19J/mm.[8]

7.2 Tracking performance

The position tracking error with nominal mass (Figure 6) was 1.9mm, and the peak velocity was 111mm/s. The performance index was thus 17.1ms for this response.

However, tracking performance varies from one movement to another and the performance index range was 13.1–30.4ms in all 20 measured responses. The performance index increased to 18.1–33.7ms when the effective inertia was 49000kg. The performance index for was about 40 ms for the four chamber cylinder,[8] and over 100 ms for the standard proportional valve.[19] When compared to the more advanced control methods,[2, 3, 4] the tracking performance is moderate only because a typical performance index is 5ms or less. The steady state position error is quite large; up to 0.7mm. Using faster valves is one way that tracking and positioning accuracy could be improved.

7.3 Comparison to the alternative controller used by Huova et al. [16]

The alternative controller studied in Huova et al.'s research [16] is based on the steady-state model of the system. An effective inertia of 49000kg was used, and the measured energy loss with the same system, trajectory and load was 15.9J/mm without tank line recovery. That is 16 percent less than in this study. The reason for this may be the different amount of crossflow used and more active control. The integral of the squared force error for one movement set was 31kN^{2}s, according to Huova et al. [16] while it averaged 50.8kN^{2}s in this study. The requirements for valves are different: the controller used in this paper requires 10ms or faster valves while the alternative controller manages with 20ms valves. Other differences between the controllers are that

the controller studied in this paper considers robustness and does not need differentiation of velocity.

8 Conclusions

The experimental results show that the combination of excellent energy efficiency and robustness, with reasonable tracking performance is possible using the suggested multi-pressure approach and model-based force control. The measured energy loss is 18.9J/mm, which is 58% lower than that achieved with a load sensing system and a mobile proportional valve. The tracking performance could be better, but it must be pointed out that the results of this paper were obtained with fixed-parameter linear controllers in the outer-loop, with relatively slow on/off valves, without throttling control and with high robustness against system uncertainties.

When compared to the alternative controller used by Huova et al.,[16] it can be concluded that the new controller does not improve energy efficiency or the force tracking performance. This is somewhat conflicting result, because faster valves and more advanced control algorithm were used. One possible reason is that the dynamic model of Eq. 1 is not accurate enough, because it does not include pipeline dynamics. The system should be redesigned using manifold technology instead of separate hosing in order to validate this assumption.

The results show that the hybrid actuator approach, in which an accumulator is integrated into the actuator and pressures are generated locally by the converter cylinders, is viable. Off the shelf components can be used, but faster valves would improve the tracking performance and reduce force ripple. There is also considerable room to improve the mechanical design in order to achieve a practical and compact solution. System-level cost comparisons should also be made in order to evaluate the competitiveness of the approach.

Declaration of Conflicting Interests

The authors declare that there is no conflict of interest.

Funding

The research was funded by the Academy of Finland (grant number 278464).

Nomenclature

A_A	Piston area, A-side (m^2)
A_B	Piston area, B-side (m^2)
$B_{eff,A}$	Effective bulk modulus of A-chamber (Pa)
$\hat{B}_{eff,A}$	Estimate of effective bulk modulus of A-chamber (Pa)

$B_{eff,B}$	Effective bulk modulus of B-chamber (Pa)
$\hat{B}_{eff,B}$	Estimate of effective bulk modulus of B-chamber (Pa)
B_h	Bulk modulus of hose (Pa)
B_{oil}	Bulk modulus of oil (Pa)
$\hat{B}_{oil}$	Estimate of bulk modulus of oil (Pa)
d	Actual time delay (s)
d_{min}	Minimum time delay (s)
E_{loss}	Energy loss during one sampling period (J)
F_{load}	Load force (N)
F_{ref}	Force reference (N)
F_{μ}	Friction force (N)
$G_F(s)$	Transfer function of the force dynamics
$G_{N,pos}(s)$	Nominal transfer function of the position loop
$G_{N,vel}(s)$	Nominal transfer function of the velocity loop
$G_P(s)$	Transfer function of the position controller

$G_{T,pos}(s)$	True transfer function of the position loop
$G_{T,vel}(s)$	True transfer function of the velocity loop
$G_V(s)$	Transfer function of the velocity controller
h	Step size of numerical integration (s)
J	Value of the cost function (N)
k_i	Coefficients of the Heun's method (Pa/s)
$K_{I,pos}$	Gain of the position controller, I-term (s^{-2})
$K_{P,pos}$	Gain of the position controller, P-term (s^{-1})
$K_{P,vel}$	Gain of the velocity controller (N s m^{-1})
$K_{v,A1,i}$	Flow coefficient of the first valve from supply pressure *i* to A-chamber ($m^3 s^{-1} Pa^{-0.5}$)
$K_{v,A2,i}$	Flow coefficient of the second valve from supply pressure *i* to A-chamber ($m^3 s^{-1} Pa^{-0.5}$)
$K_{v,B1,i}$	Flow coefficient of the first valve from supply pressure *i* to B-chamber ($m^3 s^{-1} Pa^{-0.5}$)
$K_{v,B2,i}$	Flow coefficient of the second valve from supply pressure *i* to B-chamber ($m^3 s^{-1} Pa^{-0.5}$)

N_{sw}	Number of valve switches needed to shift to the new state
m	Effective inertia (kg)
m_{min}	Minimum effective inertia (kg)
p_A	Pressure in A-chamber (Pa)
$\hat{p}_A$	Estimate of A-pressure after one sampling period (Pa)
p_B	Pressure in B-chamber (Pa)
$\hat{p}_B$	Estimate of B-pressure after one sampling period (Pa)
p_{min}	Lowest allowed chamber pressure (Pa)
p_{max}	Highest allowed chamber pressure (Pa)
$\mathbf{p_P}$	Vector of supply pressures (Pa)
$p_{P,i}$	Supply pressure i (Pa)
$Q_{A,i}$	Flow rate from supply pressure i towards A-chamber (m^3/s)
$Q_{B,i}$	Flow rate from supply pressure i towards B-chamber (m^3/s)
$Q_{conv,i}$	Calculated flow rate towards converter piston i (m^3/s)
$\mathbf{SS_A}$	Search space for A-side valves
$\mathbf{SS_B}$	Search space for B-side valves

T_S	Sampling period (s)
$T_{S,fast}$	Faster sampling period used in data collection and filtering (s)
$\mathbf{u_A}$	Vector of control signals of A-side valves
$\mathbf{u_B}$	Vector of control signals of B-side valves
v_{ref}	Velocity reference (m)
v_{tol}	Stopping tolerance for velocity reference (m)
$V_{h,A}$	Hose volume, A-side (m^3)
$V_{h,B}$	Hose volume, B-side (m^3)
$V_{0,A}$	Dead volume, A-side (m^3)
$V_{0,B}$	Dead volume, B-side (m^3)
W_{conv}	Weight for piston positions of the converter cylinders (N/m^3)
W_{loss}	Weight for energy losses (N/J)
W_{sw}	Weight for valve switching (N)
x	Piston position (m)
x_i	Piston position of the converter cylinder i (m)
x_{max}	Piston stroke (m)

x_{ref}	Reference for piston position (m)
x_{tol1}	Stopping tolerance for position error (m)
x_{tol2}	Stopping tolerance for position error (m)
$\Delta_{pos}(s)$	Multiplicative modelling error of the position loop
$\Delta_{vel}(s)$	Multiplicative modelling error of the velocity loop
τ	Tuning parameter of the position controller (s)
τ_A	Time constant of A-pressure (s)
τ_B	Time constant of B-pressure (s)
ω	Tuning parameter of the position controller (rad/s)
ξ	Tuning parameter of the position controller

References

1. Mattila J, Koivumäki J, Caldwell D and Semini C. A survey on control of hydraulic robotic manipulators with projection to future trends. *IEEE/ASME Trans. Mechatron* 2017. DOI: 10.1109/TMECH.2017.2668604

2. Kim W, Won D and Tomizuka M. Flatness-based nonlinear control for position tracking of electrohydraulic systems. *IEEE/ASME Trans. Mechatron* 2015; 20: 197–206.
3. Koivumäki J and Mattila J. High performance nonlinear motion/force controller design for redundant hydraulic construction crane automation. *Autom Constr* 2015; 51: 59–77.
4. Won D, Kim W, Shin D and Chung C. High-gain disturbance observer-based backstepping control with output tracking error constraint for electro-hydraulic systems. *IEEE Trans. Control Syst. Technol* 2015; 23: 787–795.
5. Linjama M, Huova M and Huhtala K. Model-based force and position tracking control of an asymmetric cylinder with a digital hydraulic valve. *Int. J. Fluid Power* 2016; 17: 163–172.
6. Linjama M, Huova M, et al. High-performance digital hydraulic tracking control of a mobile boom mockup. In: *10th International Fluid Power Conference (10. IFK),* Dresden, Germany, 8–10 March 2016, paper no. A-1, pp.12. Dresden: Technische Universität Dresden.
7. Eriksson B and Palmberg J-O. Individual metering fluid power systems: challenges and opportunities. *Proc Inst Mech Eng I J Syst Control Eng* 2011; 255: 196-211.
8. Linjama M, Vihtanen H-P, Sipola A and Vilenius M. Secondary controlled multi-chamber hydraulic cylinder. In: *The 11th Scandinavian International Conference*

on Fluid Power, Linköping, Sweden, 2–4 June 2009, pp.15. Linköping: Linköping University.

9. Huova M, Laamanen A and Linjama M. Energy efficiency of three-chamber cylinder with digital valve system. *Int. J. Fluid Power*, 2010; 11: 15–22.
10. Heemskerk E, Bonefeld R and Buschmann H. Control of a semi-binary hydraulic four-chamber cylinder. In: *The Fourteenth Scandinavian International Conference on Fluid Power*, Tampere, Finland, 20–22 May 2015, pp.12. Tampere: Tampere University of Technology.
11. Lumkes J and Andruch, J III. Hydraulic circuit for reconfigurable and efficient fluid power systems. In: *The Twelfth Scandinavian International Conference on Fluid Power*, Tampere, Finland, 18–20 May 2011, pp. 83–98 (Vol 2). Tampere: Tampere University of Technology.
12. Ketonen M, Linjama M and Huhtala K. Retrofitting digital hydraulics – an analytical study. In: *The 9th International Fluid Power Conference*, Aachen, Germany, 24–26 March 2014, pp.12. Aachen: RWTH Aachen University.
13. Vukovic M, Leifeld R and Murrenhoff H. STEAM – a hydraulic hybrid architecture for excavators. In: *10th International Fluid Power Conference (10. IFK)*, Dresden, Germany, 8–10 March 2016, paper no. 10-1, pp.12. Dresden: Technische Universität Dresden.

14. Linjama M, Huova M, Pietola M, et al. Hydraulic hybrid actuator: theoretical aspects and solution alternatives. In: *The Fourteenth Scandinavian International Conference on Fluid Power*, Tampere, Finland, 20–22 May 2015, pp.11. Tampere: Tampere University of Technology.
15. Huova M, Aalto A, Linjama M, Huhtala K and Pietola M. Digital hydraulic multi-pressure actuator – the concept, simulation study and first experimental results. *Int. J. Fluid Power* 2017. DOI: 10.1080/14399776.2017.1302775.
16. Huova M, Aalto A, Linjama M and Huhtala K. Study of energy losses in digital hydraulic multi-pressure actuator. In: *The 15th Scandinavian International Conference on Fluid Power*, Linköping, Sweden, 7–9 June 2017, pp.10. Linköping: Linköping University.
17. Green M and Limebeer D. *Linear robust control*. Englewood Cliffs: Prentice Hall, 1995.
18. Harrison A and Stoten D. Generalized finite difference methods for optimal estimation of derivatives in real-time control problems. *Proc Inst Mech Eng I J Syst Control Eng* 1995; 209: 67–78.
19. Linjama M, Huova M, Bostöm P, et al. Design and implementation of energy saving digital hydraulic control system. In: *The Tenth Scandinavian International Conference on Fluid Power*, Tampere, Finland, 21–23 May 2007, pp.341–359 (Vol. 2). Tampere: Tampere University of Technology.